Efficient calibration of four wheel industrial AGVs

Efficient Calibration of Four Wheel Industrial AGVs

Francesco Galasso[a,b], Dario Lodi Rizzini[a,c,*], Fabio Oleari[b], Stefano Caselli[a,c]

[a] *Robotics and Intelligent Machines Laboratory, Department of Engineering and Architecture, University of Parma, 43124, Italy*
[b] *Elettric80 S.p.A. 42030, Viano (RE), Italy*
[c] *Centro Interdipartimentale per lenergia e lambiente (CIDEA), University of Parma, 43124, Italy*

Abstract

In this paper, we propose a novel method for extrinsic and intrinsic automatic calibration of four wheel industrial Automated Guided Vehicles (AGVs) compliant with Ackermann and Dual Drive kinematics. For each kinematic model the algorithm estimates the trajectories measured by an on-board sensor and the expected ones given the state of the wheels. The estimation exploits the model equations derived in this work which constrain calibration parameters and measurements from wheel encoders and sensor odometry. The parameter values are computed through closed-form solutions of least-square estimation. The method has been implemented on Programmable Logic Controllers and tested on industrial AGVs. The developed procedure computes the parameters in about $10-15$ minutes, a significant improvement compared with one hour or more required by manual AGV calibration. Experiments with AGVs of various sizes in a warehouse have assessed the accuracy and stability of the proposed approach. The position accuracy achieved by AGVs calibrated with the proposed method is higher than the one achieved by manual calibration.

Keywords: Industrial AGVs, calibration, mobile robots.

1. Introduction

Automated Guided Vehicles (AGVs) are commonly used to transport goods and to efficiently handle logistics of industrial warehouses. Industrial AGVs are usually equipped with forks or other grasping devices for transportation of goods, and with one or more exteroceptive sensors to detect obstacles and to estimate robot position and orientation. Each vehicle must be able to localize in the environment, to perform navigation, and to precisely reach the operation points with the forklift to lay down or carry pallets. Accurate robot positioning

*Corresponding author
Email addresses: galasso.f@elettric80.it (Francesco Galasso), dario.lodirizzini@unipr.it (Dario Lodi Rizzini), oleari.f@elettric80.it (Fabio Oleari), stefano.caselli@unipr.it (Stefano Caselli)

Figure 1: An industrial Ackermann AGV with visible front steering and actuated wheels, its back forklift and a navigation laser scanner at the top of a telescopic pole. Although with slightly different mechanical structure, Dual Drive AGVs have a similar appearance.

depends on accurate odometry and sensor-based localization, which in turn requires suitable calibration. AGV calibration is the estimation of *intrinsic parameters*, which relate the wheel commands to the motion of the AGV, and *extrinsic parameters*, which define the pose of the sensor placed on the robot and used for localization. Examples of intrinsic parameters include those used in the computation of odometry like the wheel steering offsets and the wheel driving scales relating encoders and travelled distance. Examples of extrinsic parameters include the relative position and orientation of the on-board sensors w.r.t. the robot frame. In industrial practice, calibration parameters are often evaluated by iteratively correcting parameter values until the desired motion is obtained. Such calibration process requires from half an hour to one hour and half for each AGV and its accuracy largely depends on the skills and experience of the operator performing the calibration. Consistency of manual calibration with multiple, possibly different AGVs operating in the same warehouse is often hard to guarantee, which can result in different behavior when reaching the operating points.

In this paper, we propose a novel algorithm for intrinsic and extrinsic calibration of four wheel AGVs, and specifically Ackermann and Dual Drive kinematic models. Four wheel AGVs are increasingly preferred in industrial applications over simpler kinematic configurations due to their better load distribution and stability on rough grounds, as well as because of their actuation redundancy and more precise fork operations. Figure 1 shows an example of Ackermann AGV.

Both Ackermann and Dual Drive models have steering front wheels and non-steering rear wheels. In Ackermann AGVs the two front wheels are actuated, whereas in Dual Drive models the rear wheels are actuated. In Dual Drive AGVs the actuators are closer to the fork-lift on the rear of vehicles, which makes these vehicles more effective in cargo operations. To date, no suitable automated calibration procedure has been proposed for four wheel AGVs. This work stems from a joint industry-academia project aiming at improving calibration accuracy and reducing calibration time through automatic procedures. Moreover, the developed solution for calibration must take into account the software limitations of standard embedded industrial controllers (e.g. programmable logic controllers) adopted in AGVs.

Research has addressed several formulations of calibration problems for different robotic systems, including the calibration of multi-sensor systems and robot odometry [1–33]. In industrial scenarios, calibration is required for the correct operation of wheel mobile robots [2, 3, 9, 11, 34, 35], multi-tractor vehicles with specific kinematics [33], and sensor-based object grasping using manipulators [21–24]. Several of these works investigate either intrinsic or extrinsic calibration: some techniques are focused on robot intrinsic kinematics [3, 4, 7–9, 11], whereas other are designed for multi-sensor systems [15, 21, 22, 24, 30–32]. Recently, Censi et al. [1] proposed a complete calibration algorithm for robots with differential drive kinematics and equipped with a sensor. However, the kinematic model, the selection of parameters and the presented experimental validation are mostly suited for a laboratory robotic platform rather than industrial vehicles. Most of the odometry calibration literature is committed to differential drive robots. The popularity of differential drive actuation system is due to its simplicity. However, the industrial AGVs employed in transportation of heavy loads require robot kinematics with higher number of wheels. Our previous work [2] illustrated a calibration algorithm for tricycle robots, a configuration adopted in earlier design of industrial AGVs, but which is often replaced by four wheel AGVs in new automated warehouses. There are relatively few works on the calibration four wheel robots. McKerrow et al. [36] present a semi-automatic procedure computing driving scales and steering offsets, under the assumption that wheels are already aligned. The procedure proposed in [37] estimates step by step the pose of a range finder mounted on an ominidirectional robot using segment features, the gyroscope orientation and the odometric parameters. None of these method optimizes all the calibration parameters of a four wheel AGV in a single step. Maye et al. [38] proposed a general calibration framework that can estimates all kind of parameters, intrinsic or extrinsic, provided a model. The main advantages of such method are its applicability for online calibration and the automatic numerical evaluation of observability. However, since it is designed for general AGV models, it is based on numerical methods and model approximations (e.g. linearization, covariance projection based on Jacobian, etc.), and online continous calibration may suffer from outlier measurements in the case of industrial AGVs with lifelong operability. In order to achieve the high position accuracy required in industrial applications, it would be convenient to evaluate all the calibration parameters of four wheel

AGVs by optimizing an objective function depending on all the measurements. Unfortunately, four wheel models are over-actuated and intrinsic kinematic parameters cannot be identified by means of the observed trajectory.

This work develops a complete calibration procedure of four wheel AGVs according to the principle adopted in [1, 2]: the comparison of the trajectory measured by the on-board sensor and the expected trajectory of the AGV. Due to the observability issues of four wheel kinematic models, the only precondition is the manual alignment of the front wheels of the robot. To observe trajectories, the robot must be equipped with on-board sensors enabling egomotion estimation. Sensors with such capability, like range finders, are usually mounted on industrial AGVs and other mobile robots for localization and navigation as well as obstacle detection. The expected trajectories also depend on odometry and, thus, on intrinsic parameters. These different measurements are encoded by a set of constraints among intrinsic and extrinsic parameters, which are exploited to perform least-square estimation. In the Ackermann and Dual Drive kinematic models addressed in this paper, the presence of multiple independently actuated wheels makes calibration more difficult as well as crucial to limit slipping and to achieve consistent motion of all actuators. The main contribution of this paper is the derivation of equations for four wheel Ackermann and Dual Drive kinematics, and their closed-form solutions. The intrinsic calibration equations accurately describe the real motion of AGVs under the assumption of wheel alignment and negligible wheel slipping. The presented extrinsic calibration algorithm extends our previous work on tricycle AGVs [2]. Moreover, the proposed closed-form solution is suitable for implementation on PLCs (Programmable Logic Controllers) used for industrial AGVs. The second contribution of the paper is the implementation, deployment and assessment of the proposed methods on industrial AGVs. In particular, the implemented application enables full estimation of calibration parameters in about $10 - 15$ minutes. Repeated calibration trials have exhibited numerical stability and precision in the values of computed parameters. Positioning tests on actual AGVs have also demonstrated the higher accuracy of the proposed calibration algorithm w.r.t. manual calibration.

The paper is organized as follows. Section 2 presents the general model of four wheel AGVs and the specific equations of Ackermann and Dual Drive robots. Sections 3 and 4 illustrate the solutions to respectively intrinsic and extrinsic calibration. Section 5 discusses practical implementation and deployment of calibration algorithms on industrial AGVs. Section 6 presents the results about calibration repeatability and position precision. Finally, section 7 concludes the paper.

2. Problem Formulation

This section illustrates the *Ackermann* and *Dual Drive* kinematics and provides the formulation of their intrinsic parameter estimation. These two models have four wheels and are both over-actuated vehicles, since there are more actuators than the system degrees-of-freedom. Thus, large wheel slipping may occur

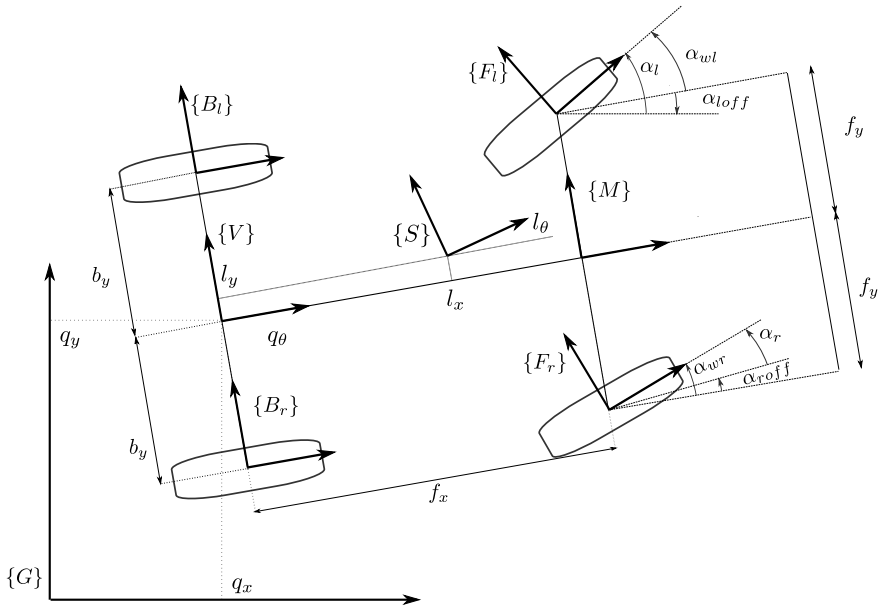

Figure 2: Structure of four wheel AGVs with the reference frames of AGV and its parameters. Counterclockwise arrows refer to positive angles, whereas clockwise ones (e.g. the arrow of α_{loff}) are negative.

with arbitrary values of steering and speed. When wheel commands yield a consistent AGV motion, i.e. correspond to the kinematics of a rigid body, these input commands are called *consistent*. When the commands are not consistent, robot dynamics must be taken into account to compute the final motion. Since accurate modelling and estimation of torques, masses and friction is difficult and beyond the scope of the work, we limit the analysis to kinematics.

2.1. Modelling Four Wheel AGVs

Figure 2 illustrates the general structure of four wheel robots with reference frames and dimensional parameters. All the reference frames are treated in the following as either tridimensional frames with parallel axes $\hat{\mathbf{z}}$ or planar frames. Reference frames include a global inertial frame $\{G\}$ fixed in the environment, the robot frame $\{V\}$, the frame $\{S\}$ attached to the navigation sensor, and the wheel frames $\{F_l\}$ (front-left wheel), $\{F_r\}$ (front-right wheel), $\{B_l\}$ (back left wheel), and $\{B_r\}$ (back-right wheel). The two front wheels $\{F_l\}$ and $\{F_r\}$ have independent steering actuators controlling the respective steering angles. The dimensional parameters are the so called wheelbase f_x, i.e. the distance between front and rear axes, and the front and back wheel half-axes, respectively f_y and b_y.

The Ackermann and Dual Drive models are compliant with this geometric description. In the Ackermann model, the front wheels F_l and F_r are both

steering and actuated whereas the rear wheels B_l and B_r are passive. The rolling speed of passive wheels is completely set by the other actuated wheels. In the Dual Drive model, F_l and F_r are only steering whereas B_l and B_r are actuated and not steering. The front steering-only wheels are used to guide the vehicle and to limit slipping.

Since all the frames belong to a rigid body, the robot configuration in planar space can be described by a unique pose vector $\mathbf{q} = [q_x, q_y, q_\theta]^\top \in \mathrm{se}(2)$. The state vector represents the position $\mathbf{q}_{pos} = [q_x, q_y]^\top \in \mathrm{R}^2$ and orientation $q_\theta \in \mathrm{so}(2)$ of reference frame $\{V\}$ w.r.t. the global frame $\{G\}$. Henceafter, the subscript $\cdot_{pos}$ applied to a pose vector refers to its position coordinate vector in $\mathbb{R}^2$. The reference frame $\{V\}$ is sometimes called logical point, since robot state is logically represented as a point particle located in the origin of this frame. The general kinematic equation describing the evolution of state vector $\mathbf{q}$ over time is

$$\dot{\mathbf{q}} = \begin{bmatrix} v_{lp} \cos(q_\theta) \\ v_{lp} \sin(q_\theta) \\ \omega_{lp} \end{bmatrix} \tag{1}$$

The input controls of eq. (1) are given by the linear and angular velocities v_{lp} and ω_{lp} of the logical point. It is sometimes convenient to express the linear and angular speeds of robot frame $\{V\}$ from global frame $\{G\}$ in $\{V\}$ 3D coordinates as

$${}^V\mathbf{v}_{V,G} = \begin{bmatrix} v_{lp} & 0 & 0 \end{bmatrix}^\top \tag{2}$$

$${}^V\boldsymbol{\omega}_{V,G} = \begin{bmatrix} 0 & 0 & \omega_{lp} \end{bmatrix}^\top \tag{3}$$

Observe that ${}^V\mathbf{v}_{V,G}$ has only a longitudinal component aligned with axis $\hat{\mathbf{x}}_V$ of frame $\{V\}$, and zero lateral velocity. Odometry is obtained by integration of equation (1) over a given time interval. The exact expression is straightforwardly obtained under the assumption that input controls v_{lp} and ω_{lp} are constant over $[t_{k-1}, t_k]$. Thus, the curvature radius $r_\kappa^k = v_{lp}/\omega_{lp}$ is also constant and the robot performs a circular path. The analytical expression of robot relative motion $\boldsymbol{\delta}^k = [{\boldsymbol{\delta}_{pos}^k}^\top, \delta_\theta^k]^\top = [\delta_x^k, \delta_y^k, \delta_\theta^k]^\top \in \mathrm{se}(2)$ is given by

$$\begin{aligned} \boldsymbol{\delta}_{pos}^k &= \mathbf{R}(-q_\theta(t_{k-1})) \ (\mathbf{q}_{pos}(t_k) - \mathbf{q}_{pos}(t_{k-1})) \\ &= r_\kappa^k \begin{bmatrix} \sin(\delta_\theta^k) \\ 1 - \cos(\delta_\theta^k) \end{bmatrix} \end{aligned} \tag{4}$$

$$\delta_\theta^k = q_\theta(t_k) - q_\theta(t_{k-1}) = \int_{t_{k-1}}^{t_k} \omega_{lp} \, d\tau \tag{5}$$

Equations (4) and (5) provide the exact expression of the relative motion over circular path segments.

Physically, the values of the velocities v_{lp} and ω_{lp} of the robot logical point depend on the robot wheels. The forward kinematic model consists of the equations relating the wheel steering angles and rolling speeds to the logical point velocities. The parameters used in forward kinematic model are called

intrinsic parameters. In section 2.2, we illustrate the forward kinematic models and the intrinsic parameters of Ackermann and Dual Drive models.

The robot is equipped with a sensor, which allows navigation and egomotion estimation. In the case of industrial AGVs, this sensor is usually a planar sensor like a laser scanner specifically designed to localize the robot in the environment by detecting artificial landmarks. The range finder mounted on the robot is such that the scanning plane is parallel to the ground plane. Thus, the position and orientation of sensor frame $\{S\}$ w.r.t. the robot frame $\{V\}$ is described by the planar pose vector $\mathbf{l} = [l_x, l_y, l_\theta]^\top \in \mathrm{se}(2)$. The parameters $\mathbf{l}$ that encode the sensor pose w.r.t. to the vehicle are called *extrinsic parameters*. Accurate estimation of extrinsic parameters is needed to perform robot localization and navigation using the sensor. The measurements acquired from the sensor enable the estimation of relative motion $\boldsymbol{\zeta}^k = [\zeta_x^k, \zeta_y^k, \zeta_\theta^k]^\top \in \mathrm{se}(2)$ of frame $\{S\}$ over time interval $[t_{k-1}, t_k]$. In the case of laser scanner, the value $\boldsymbol{\zeta}^k$ is computed using registration algorithms [39].

The simultaneous estimation of intrinsic and extrinsic calibration parameters is performed through the comparison of the odometry $\boldsymbol{\delta}^k$ and the sensor egomotion $\boldsymbol{\zeta}^k$ over several path segments $k = 1, \ldots, n$. The value of $\boldsymbol{\delta}^k$ depends on the intrinsic parameters of the robot through forward kinematics as illustrated in section 2.2. On the other hand, $\boldsymbol{\delta}^k$ and $\boldsymbol{\zeta}^k$ are constrained by the extrinsic parameters $\mathbf{l}$ through the following relation

$$\begin{bmatrix} \mathbf{l}_{pos} + \mathbf{R}(l_\theta)\,\boldsymbol{\zeta}_{pos}^k \\ l_\theta + \zeta_\theta^k \end{bmatrix} = \begin{bmatrix} \boldsymbol{\delta}_{pos}^k + \mathbf{R}\left(\delta_\theta^k\right)\mathbf{l}_{pos} \\ \delta_\theta^k + l_\theta \end{bmatrix} \tag{6}$$

The symbol $\mathbf{R}(\cdot)$ refers, henceafter, both to the map from an angle $\beta \in S^1$ to the corresponding rotation matrix of $\mathbf{R}(\beta) \in \mathrm{SO}(2)$ and to the map from a vector $b \in \mathbb{R}^2$ to a skew matrix $\mathbf{R}(b) \in \mathbb{R}^{2\times 2}$ defined respectively as

$$\mathbf{R}(\beta) \triangleq \begin{bmatrix} \cos\beta & -\sin\beta \\ \sin\beta & \cos\beta \end{bmatrix}, \mathbf{R}(b) \triangleq \begin{bmatrix} b_x & -b_y \\ b_y & b_x \end{bmatrix} \tag{7}$$

The angular part of eq. (6) implies that the relative rotation angles of the robot and of the sensor attached as a rigid body are equal: $\delta_\theta^k = \zeta_\theta^k$. Since forward kinematics can relate the input control and intrinsic parameters to each δ_θ^k, this equation will be used to solve intrinsic calibration. The position part of eq. (6) constrains $\boldsymbol{\delta}_{pos}^k$ (computed from controls and intrinsic parameters) and $\boldsymbol{\zeta}_{pos}^k$ (directly measured using sensor registration) with the extrinsic parameters $\mathbf{l}$. The difference between the two members of equation (6) can be interpreted as an error vector $\mathbf{e}_k$ dependent from $\mathbf{l}$. Thus, the value of $\mathbf{l}$ can be computed by least-square estimation over errors $\mathbf{e}_k$ for all path segments $k = 1, \ldots, n$.

2.2. Forward Kinematics of Four Wheel AGVs

The velocities of logical point are related to the velocities set by the wheels. The relations between speeds can be computed under the hypothesis that the

robot can be treated as a rigid body. In particular, we can use the *wheel equation* [40] applied to each wheel frame $\{W\}$

$$^{V}\mathbf{v}_{W,G} = {}^{V}\mathbf{v}_{V,G} + {}^{V}\boldsymbol{\omega}_{V,G} \times {}^{V}\mathbf{p}_{W} \tag{8}$$

where W is either F_l, F_r, B_l or B_r. The resulting velocities at the four wheels in robot coordinates are obtained through the substitution of eq. (2), (3) and the position vector of each wheel (see the parameters in Figure 2) in equation (8) as

$$^{V}\mathbf{v}_{F_l,G} = \begin{bmatrix} v_{lp} - \omega_{lp} f_y & \omega_{lp} f_x & 0 \end{bmatrix}^{\top} \tag{9}$$

$$^{V}\mathbf{v}_{F_r,G} = \begin{bmatrix} v_{lp} + \omega_{lp} f_y & \omega_{lp} f_x & 0 \end{bmatrix}^{\top} \tag{10}$$

$$^{V}\mathbf{v}_{B_l,G} = \begin{bmatrix} v_{lp} - \omega_{lp} b_y & 0 & 0 \end{bmatrix}^{\top} \tag{11}$$

$$^{V}\mathbf{v}_{B_r,G} = \begin{bmatrix} v_{lp} + \omega_{lp} b_y & 0 & 0 \end{bmatrix}^{\top} \tag{12}$$

The above equations provide the velocity required for each wheel in order to achieve the desired velocities v_{lp} and ω_{lp} in the logic point.

However, each actuated wheel is controlled by its rolling speed and, for steering wheels, by its steering angle through actuators. We describe the parameters that enable setting of wheel velocities referred to the four wheel robot illustrated in Figure 2.

- *Steering offsets.* The two front wheels are steering and their steering angles α_{wl} and α_{wr} are referred to the forward direction of robot corresponding to axis $\hat{\mathbf{x}}_V$ of frame $\{V\}$. The steering motors control the steering angles and their encoders measure the angles α_l and α_r w.r.t. the steer encoder reference. Ideally, the steer encoder references should be aligned with the forward direction of robot, i.e. axis $\hat{\mathbf{x}}_V$ of frame $\{V\}$. In practice, there are *steering offsets* α_{loff} and α_{roff} of encoders such that

$$\alpha_{wl} = \alpha_l + \alpha_{loff} \qquad\qquad \alpha_{wr} = \alpha_r + \alpha_{roff} \tag{13}$$

- *Driving scales.* The distance travelled by an actuated wheel is proportional to its turning angle. Physically, the turning angle over a time interval $[t_{k-1}, t_k]$ is measured by counting the corresponding tick number of the wheel encoder n_w^k. The driving scale s_w is the parameter that relates the relative encoder tick n_w^k to the travelled distance $s_w n_w^k$ (e.g. in mm). The corresponding wheel velocity at time t is denoted as $s_w \dot{n}_w(t)$. In the Ackermann model, the left and right front wheels are actuated and the module of their velocities is equal respectively to

$$\|{}^{V}\mathbf{v}_{F_l,G}\| = s_{wl}\dot{n}_{wl} \qquad\qquad \|{}^{V}\mathbf{v}_{F_r,G}\| = s_{wr}\dot{n}_{wr} \tag{14}$$

  where s_{wl} and s_{wr} represent respectively the left and right driving scales, and $\dot{n}_{wl}$ and $\dot{n}_{wl}$ are the turning rates of left and right wheels measured

in encoder ticks. In the Dual Drive model, the same notation is adopted for the rear wheels

$$\|^V \mathbf{v}_{B_l,G}\| = s_{wl}\dot{n}_{wl} \qquad \|^V \mathbf{v}_{B_r,G}\| = s_{wr}\dot{n}_{wr} \tag{15}$$

where s_{wl}, s_{wr}, $\dot{n}_{wl}$ and $\dot{n}_{wl}$ refer to the rear wheels. The physical meaning of these quantities, i.e. whether referred to front or back wheels, will be clear from the context.

Forward kinematics consist of the equations relating the logical point velocities to the wheel controls. Forward kinematics depend on the *intrinsic parameters* α_{loff}, α_{roff}, s_{wl} and s_{wr} discussed above. The goal of intrinsic calibration is the estimation of such parameters. We derive the equations that relate the velocities of the robot logical point and the velocities of the wheels for Ackermann and Dual Drive models.

Ackermann model. In the Ackermann model, the two front wheels are steering and actuated, whereas the rear wheels are passive and not controlled. Its forward kinematics is obtained by comparing the velocities of frames $\{F_l\}$ and $\{F_r\}$, from eq.(9)-(10), with the wheel velocities in eq. (14) as

$${}^V\mathbf{v}_{F_l,G} = \begin{bmatrix} s_{wl}\ \dot{n}_{wl}\,\mathrm{c}\,\alpha_{wl} \\ s_{wl}\ \dot{n}_{wl}\,\mathrm{s}\,\alpha_{wl} \\ 0 \end{bmatrix} = \begin{bmatrix} v_{lp} - \omega_{lp} f_y \\ \omega_{lp} f_x \\ 0 \end{bmatrix} \tag{16}$$

$${}^V\mathbf{v}_{F_r,G} = \begin{bmatrix} s_{wr}\ \dot{n}_{wr}\,\mathrm{c}\,\alpha_{wr} \\ s_{wr}\ \dot{n}_{wr}\,\mathrm{s}\,\alpha_{wr} \\ 0 \end{bmatrix} = \begin{bmatrix} v_{lp} + \omega_{lp} f_y \\ \omega_{lp} f_x \\ 0 \end{bmatrix} \tag{17}$$

where the modules of wheel velocities in eq. (14) are projected according to steering angles α_{wl} and α_{wr}. Forward kinematics of Ackermann model is given by

$$v_{lp} = \frac{s_{wl}\dot{n}_{wl}\,\mathrm{c}\,\alpha_{wl} + s_{wr}\dot{n}_{wr}\,\mathrm{c}\,\alpha_{wr}}{2} \tag{18}$$

$$\omega_{lp} = \frac{s_{wl}\ \dot{n}_{wl}\,\mathrm{s}\,\alpha_{wl}}{f_x} \tag{19}$$

$$\omega_{lp} = \frac{s_{wr}\ \dot{n}_{wr}\,\mathrm{s}\,\alpha_{wr}}{f_x} \tag{20}$$

$$\omega_{lp} = \frac{s_{wr}\ \dot{n}_{wr}\,\mathrm{c}\,\alpha_{wr} - s_{wl}\ \dot{n}_{wl}\,\mathrm{c}\,\alpha_{wl}}{2f_y} \tag{21}$$

Since Ackermann AGVs are over-actuated, there are multiple expressions for ω_{lp}. The values of independent controls α_l, α_r, $\dot{n}_{wl}$ and $\dot{n}_{wr}$ must be chosen s.t. equations (18)-(21) are simultaneously satisfied. Otherwise, kinematics is insufficient to model wheel slipping and system dynamics must be taken into account to predict its evolution.

Dual Drive model. Dual Drive AGVs have two front steering wheels and two rear actuated wheels, which cannot steer. The same procedure adopted for

the Ackermann model can be applied to compute Dual Drive forward kinematics. The velocities ${}^{V}\mathbf{v}_{B_l,G}$ and ${}^{V}\mathbf{v}_{B_r,G}$ of rear wheels have only longitudinal components along axis $\hat{\mathbf{x}}_V$, that are equal to

$$s_{wl}\ \dot{n}_{wl} = v_{lp} - \omega_{lp} b_y \tag{22}$$

$$s_{wr}\ \dot{n}_{wr} = v_{lp} + \omega_{lp} b_y \tag{23}$$

Such equations can be used to compute the forward kinematics of Dual Drive

$$v_{lp} = \frac{s_{wl}\ \dot{n}_{wl} + s_{wr}\ \dot{n}_{wr}}{2} \tag{24}$$

$$\omega_{lp} = \frac{s_{wr}\ \dot{n}_{wr} - s_{wl}\ \dot{n}_{wl}}{2b_y} \tag{25}$$

Driving scales s_{wl} and s_{wr} are the only intrinsic parameters appearing in the above relations. The steering angles are required for the steering passive wheels described by

$${}^{V}\mathbf{v}_{F_l,G} = \begin{bmatrix} v_{fl}\,\mathrm{c}\,\alpha_{wl} \\ v_{fl}\,\mathrm{s}\,\alpha_{wl} \\ 0 \end{bmatrix} = \begin{bmatrix} v_{lp} - \omega_{lp} f_y \\ \omega_{lp} f_x \\ 0 \end{bmatrix} \tag{26}$$

$${}^{V}\mathbf{v}_{F_r,G} = \begin{bmatrix} v_{fr}\,\mathrm{c}\,\alpha_{wr} \\ v_{fr}\,\mathrm{s}\,\alpha_{wr} \\ 0 \end{bmatrix} = \begin{bmatrix} v_{lp} + \omega_{lp} f_y \\ \omega_{lp} f_x \\ 0 \end{bmatrix} \tag{27}$$

In equations (26) and (27) the modules of wheel velocities, respectively v_{fl} and v_{fr} for front left and right wheels, are not set by motor commands. These equations can be manipulated to write two constraints, one for each front wheel, according to the following procedure (described for the front left wheel, but similar for the right one). We can remove the dependence from v_{fl} by multiplying the x and y component of eq. (26) by respectively $\mathrm{s}\,\alpha_{wl}$ and $\mathrm{c}\,\alpha_{wl}$. Then, the two equations are subtracted member by member. Finally, the values of v_{lp} and ω_{lp} from equations (24) and (25) can be substituted. The final result is the following:

$$\begin{aligned} 0 = & \frac{s_{wl}\ \dot{n}_{wl} + s_{wr}\ \dot{n}_{wr}}{2}\ \mathrm{s}\,\alpha_{wl} \\ & + \frac{s_{wr}\ \dot{n}_{wr} - s_{wl}\ \dot{n}_{wl}}{2b_y}\ (-f_y\,\mathrm{s}\,\alpha_{wl} - f_x\,\mathrm{c}\,\alpha_{wl}) \end{aligned} \tag{28}$$

$$\begin{aligned} 0 = & \frac{s_{wl}\ \dot{n}_{wl} + s_{wr}\ \dot{n}_{wr}}{2}\ \mathrm{s}\,\alpha_{wr} \\ & + \frac{s_{wr}\ \dot{n}_{wr} - s_{wl}\ \dot{n}_{wl}}{2b_y}\ (f_y\,\mathrm{s}\,\alpha_{wr} - f_x\,\mathrm{c}\,\alpha_{wr}) \end{aligned} \tag{29}$$

2.3. Discussion

The model presented in the previous subsection is based on the assumption that the velocity directions and steering angles of wheels are congruent. In particular, equations (16)-(17) for Ackermann and (26)-(27) for Dual Drive state

that vectors ${}^V\mathbf{v}_{F_l,G}$ and ${}^V\mathbf{v}_{F_r,G}$ have orientation angles α_{wl} and α_{wr}. This assumption holds only when no wheel slippage occurs and the input controls are consistent with the rigid body motion. Otherwise, since Ackermann and Dual Drive are over-actuated kinematics, the kinematic parameters cannot be identified by means of the observed trajectory. For example, the same straight motion can be obtained either with perfectly parallel wheels or with symmetrically opposite steering angles. Thus, before the calibration procedure, a manual parallelization of wheels is performed to guarantee the feasibility of such condition. The procedure is briefly described in section 5.

The wheel parallelization procedure is performed with tolerance on offset accuracy. Once the wheel are approximately aligned, the optimization methods for the two four wheel kinematics described in sections 3 and 4 can effectively estimate the calibration parameters, as shown by experiments.

3. Intrinsic Calibration

The intrinsic calibration procedures of Ackermann and Dual Drive models depend on their specific equations. Nonetheless, the principle applied in intrinsic calibration is the same. Since the AGV is a rigid body, the rotation angles of all the frames rigidly attached to the robot are the same. In order to use the simplified equations of odometry (4)-(5), only time intervals $[t_{k-1}, t_k]$ with constant control input are taken into account. The ^{k} apex notation is used henceafter for all the parameter values and the measurements related to time intervals $[t_{k-1}, t_k]$ with $k = 1, \ldots, n_k$. The path travelled over $[t_{k-1}, t_k]$ with constant wheel steering angles and velocities is called *path segment* k. In particular, for each segment k, we measure the following variables:

- the steering angles of left and right front wheels, respectively α_l^k and α_r^k, which are constant on path segment k and measured by the steering encoders;
- the left and right wheel spins n_{wl}^k and n_{wr}^k measured in encoder ticks (front wheels for Ackermann, rear wheels for Dual Drive);
- the relative rotation δ_θ^k of the AGV while following a path segment between time instant t_{k-1} and t_k.

As observed before, the relative rotation δ_θ^k is not measured directly, but obtained through sensor registration ζ_θ^k. In the industrial setup, sensor registration is performed by matching artificial landmarks made of reflective material in known positions. These landmarks are called *reflectors* and are detected by the laser scanner.

3.1. Calibration of Ackermann Model

The solution of Ackermann intrinsic calibration can be obtained by integrating equations (19)-(21), which relate angular velocity ω_{lp} to wheel parameters, over several path segments k. The three expressions of ω_{lp} can be substituted

into equation (5) and equated to $\delta_\theta^k = \zeta_\theta^k$. Moreover, we substitute the expression of total steering angles $\alpha_{wl}^k = \alpha_l^k + \alpha_{loff}$ and $\alpha_{wr}^k = \alpha_r^k + \alpha_{roff}$ and of the wheel spin angles

$$n_{wl}^k = \int_{t_{k-1}}^{t_k} \dot{n}_{wl} d\tau \quad n_{wr}^k = \int_{t_{k-1}}^{t_k} \dot{n}_{wr} d\tau \tag{30}$$

The result of this operation over path segment k consists of the three linear equations

$$\mathbf{A}_a^k \, \mathbf{x}_a = \mathbf{b}_a^k \tag{31}$$

where the matrices and vectors are defined as

$$\mathbf{x}_a = \begin{bmatrix} x_{a1} \\ x_{a2} \\ x_{a3} \\ x_{a4} \end{bmatrix}^\top = \begin{bmatrix} s_{wl}\,\mathrm{c}\,\alpha_{loff} \\ s_{wl}\,\mathrm{s}\,\alpha_{loff} \\ s_{wr}\,\mathrm{c}\,\alpha_{roff} \\ s_{wr}\,\mathrm{s}\,\alpha_{roff} \end{bmatrix} \tag{32}$$

$$\begin{aligned} \mathbf{A}_a^k &= \begin{bmatrix} \frac{n_{wl}^k\,\mathrm{s}\,\alpha_l^k}{f_x} & \frac{n_{wl}^k\,\mathrm{c}\,\alpha_l^k}{f_x} & 0 & 0 \\ 0 & 0 & \frac{n_{wr}^k\,\mathrm{s}\,\alpha_r^k}{f_x} & \frac{n_{wr}^k\,\mathrm{c}\,\alpha_r^k}{f_x} \\ \frac{-n_{wl}^k\,\mathrm{c}\,\alpha_l^k}{2f_y} & \frac{n_{wl}^k\,\mathrm{s}\,\alpha_l^k}{2f_y} & \frac{n_{wr}^k\,\mathrm{c}\,\alpha_r^k}{2f_y} & \frac{-n_{wr}^k\,\mathrm{s}\,\alpha_r^k}{2f_y} \end{bmatrix} \\ &= \begin{bmatrix} a_{slcl} & a_{slsl} & 0 & 0 \\ 0 & 0 & a_{srcr} & a_{srsr} \\ a_{clcl} & a_{clsl} & a_{crcr} & a_{crsr} \end{bmatrix} \end{aligned} \tag{33}$$

$$\mathbf{b}_a^k = \begin{bmatrix} \delta_\theta^k & \delta_\theta^k & \delta_\theta^k \end{bmatrix}^\top \tag{34}$$

The original intrinsic parameters s_{wl}, s_{wlr}, α_{loff} and α_{roff} have been conveniently substituted with other variables s.t. the equations are linear w.r.t. the new variables. Of course, additional constraints may be inserted to keep consistency, when the new variable space is a specific manifold. The above constraints are replicated for all path segments with $k = 1, \ldots, n_k$ to form the linear system with matrix $\mathbf{A}_y$ and known term vector $\mathbf{b}_y$ defined as

$$\mathbf{A}_a = \begin{bmatrix} \mathbf{A}_a^{1\top} & \mathbf{A}_a^{2\top} & \ldots & \mathbf{A}_a^{n_k\top} \end{bmatrix}^\top \tag{35}$$

$$\mathbf{b}_a = \begin{bmatrix} \mathbf{b}_a^{1\top} & \mathbf{b}_a^{2\top} & \ldots & \mathbf{b}_a^{n_k\top} \end{bmatrix}^\top \tag{36}$$

A least square solution $\mathbf{x}_a^*$ for this system can be found using *Moore-Penrose pseudoinverse*. Thus, Ackermann model calibration can be formulated as the following problem:

Problem 1 (Ackermann intrinsic calibration)**.** *Find the parameter vector* $\mathbf{x}_a^* \in \mathbb{R}^4$ *that*

$$\text{minimize} \|\mathbf{A}_a \mathbf{x}_a - \mathbf{b}_a\|^2 \tag{37}$$

where $\mathbf{A}_a$ *and* $\mathbf{b}_a$ *are given respectively by eq. (35) and (36). The final calibration parameters are computed as*

$$s^*_{wl} = \sqrt{x^2_{a1} + x^2_{a2}} \tag{38}$$

$$s^*_{wr} = \sqrt{x^2_{a3} + x^2_{a4}} \tag{39}$$

$$\alpha^*_{loff} = \text{atan2}\left(x_{a2}, x_{a1}\right) \tag{40}$$

$$\alpha^*_{roff} = \text{atan2}\left(x_{a4}, x_{a3}\right) \tag{41}$$

3.2. Calibration of Dual-Drive Model

The solution of intrinsic calibration of Dual Drive AGVs is derived with a procedure analogous to the one applied to the Ackermann model. Yet there is an important difference between the formula of ω_{lp} in eq. (25) and the constraints on steering wheels in eq.(28)-(29). The first constraint can be used to estimate the driving scales s_{wl} and s_{wr} of respectively left and right back wheels. The latter relations are used to estimate the steering offsets of left and right front wheels, respectively α_{loff} and α_{roff}. This two-step estimation (first the estimation of driving scales, followed by steering offsets) has a closed-form solution, which is suitable for implementation in embedded systems. The integration of eq. (25) leads to

$$\delta^k_\theta = \underbrace{\left(\frac{n^k_{wr}}{2b_y}\right)}_{a^k_{\omega r}} s_{wr} - \underbrace{\left(\frac{n^k_{wr}}{2b_y}\right)}_{a^k_{\omega l}} s_{wl} \tag{42}$$

where the travelled angles n^k_{wl} and n^k_{wr} are measured by the left and right wheel encoders as in section 3.1. The multiple constraints in the form of eq. (42) collected over path segments $k = 1, \ldots, n_k$ can be arranged into the linear system

$$\underbrace{\begin{bmatrix} \delta^1_\theta \\ \delta^2_\theta \\ \vdots \\ \delta^{n_k}_\theta \end{bmatrix}}_{\mathbf{b}_s} = \underbrace{\begin{bmatrix} a^1_{\omega l} & a^1_{\omega r} \\ a^2_{\omega l} & a^2_{\omega r} \\ \vdots & \vdots \\ a^{n_k}_{\omega l} & a^{n_k}_{\omega r} \end{bmatrix}}_{\mathbf{A}_s} \underbrace{\begin{bmatrix} s_{wl} \\ s_{wr} \end{bmatrix}}_{\mathbf{x}_s} \tag{43}$$

Similarly to previous case, the conditions given by the linear system in eq. (43) often do not hold simultaneously. Hence, the driving scales $\mathbf{x}_s$ are evaluated by minimizing $\|\mathbf{A}_s\mathbf{x}_s - \mathbf{b}_s\|$. Once the driving scales are evaluated, equations (28) and (29) can be integrated over all path segments k. The left steering offset α_{loff} appears only in eq. (28), while α_{roff} only in eq. (29). Thus, two sets of

independent equations in α_{loff} and α_{roff}, which can be solved independently, are obtained from the integration

$$\underbrace{\begin{bmatrix} a^1_{\alpha l,1} & a^1_{\alpha,l,2} \\ \vdots & \vdots \\ a^{n_k}_{\alpha l,1} & a^{n_k}_{\alpha,l,2} \end{bmatrix}}_{\mathbf{A}_{\alpha,l}} \cdot \underbrace{\begin{bmatrix} \mathrm{c}\,\alpha_{loff} \\ \mathrm{s}\,\alpha_{loff} \end{bmatrix}}_{\mathbf{x}_l=[x_{l1},x_{l2}]]^\top} = \mathbf{0} \tag{44}$$

$$\underbrace{\begin{bmatrix} a^1_{\alpha r,1} & a^1_{\alpha,r,2} \\ \vdots & \vdots \\ a^{n_k}_{\alpha r,1} & a^{n_k}_{\alpha,r,2} \end{bmatrix}}_{\mathbf{A}_{\alpha,r}} \cdot \underbrace{\begin{bmatrix} \mathrm{c}\,\alpha_{roff} \\ \mathrm{s}\,\alpha_{roff} \end{bmatrix}}_{\mathbf{x}_r=[x_{r1},x_{r2}]]^\top} = \mathbf{0} \tag{45}$$

where the coefficients of the two linear system matrices are defined as

$$a^k_v = \frac{s_{wl} n^k_{wl} + s_{wr} n^k_{wr}}{2} \tag{46}$$

$$a^k_\omega = \frac{s_{wr} n^k_{wr} - s_{wl} n^k_{wl}}{2 b_y} \tag{47}$$

$$a^k_{\alpha l,1} = (a^k_v - f_y a^k_\omega)\,\mathrm{s}\,\alpha^k_l - f_x a^k_\omega\,\mathrm{c}\,\alpha^k_l \tag{48}$$

$$a^k_{\alpha l,2} = (a^k_v - f_y a^k_\omega)\,\mathrm{c}\,\alpha^k_l + f_x a^k_\omega\,\mathrm{s}\,\alpha^k_l \tag{49}$$

$$a^k_{\alpha r,1} = (a^k_v - f_y a^k_\omega)\,\mathrm{s}\,\alpha^k_l - f_x a^k_\omega\,\mathrm{c}\,\alpha^k_l \tag{50}$$

$$a^k_{\alpha r,2} = (a^k_v - f_y a^k_\omega)\,\mathrm{c}\,\alpha^k_l + f_x a^k_\omega\,\mathrm{s}\,\alpha^k_l \tag{51}$$

Equations (44) and (45) have been written to highlight the linearity w.r.t. respectively vectors $\mathbf{x}_l$ and $\mathbf{x}_r$. The two variables are subject to constraints $\|\mathbf{x}_l\|^2 = 1$ and $\|\mathbf{x}_r\|^2 = 1$. Due to noise in measurements, the above conditions are usually not satisfied. The estimation of left and right steering offsets is achieved by finding the $\mathbf{x}_l$ or $\mathbf{x}_r$ that minimize respectively $\|\mathbf{A}_{\alpha,l}\mathbf{x}_l\|^2$ and $\|\mathbf{A}_{\alpha,r}\mathbf{x}_r\|^2$. Fortunately, the problem of minimizing a homogeneous quadratic function over a sphere is well-known and has a closed-form solution (see [41, p. 593]). It suffices to find the eigenvector of matrix $\mathbf{A}^\top_{\alpha,\cdot}\mathbf{A}_{\alpha,\cdot}$ corresponding to its minimum eigenvalue. The intrinsic calibration of Dual Drive model is summarized by the following problem:

Problem 2 (Dual Drive intrinsic calibration)**.** *Solve the following steps.*

1. *Find the driving scale vector* $\mathbf{x}^*_s = [s_{wl}, s_{wr}] \in \mathbb{R}^2$ *that*

$$\text{minimize} \|\mathbf{A}_s\mathbf{x}_s - \mathbf{b}_s\|^2 \tag{52}$$

$$\text{s.t.} \quad y_{s1}, y_{s2} > 0 \tag{53}$$

where $\mathbf{A}_s$ *and* $\mathbf{b}_s$ *are defined in eq. (43).*

2. *After substitution of* $\mathbf{x}_s^*$, *find* $\mathbf{x}_l^*, \mathbf{x}_r^* \in \mathbb{R}^2$

$$\mathbf{x}_l^* = \underset{\|\mathbf{x}_l\|^2=1}{\operatorname{argmin}} \|\mathbf{A}_{\alpha,l}\mathbf{x}_l\|^2 \tag{54}$$

$$\mathbf{x}_r^* = \underset{\|\mathbf{x}_r\|^2=1}{\operatorname{argmin}} \|\mathbf{A}_{\alpha,r}\mathbf{x}_r\|^2 \tag{55}$$

The values of steering offsets *are computed as*

$$\alpha_{loff}^* = \operatorname{atan2}\left(x_{l2}^*, x_{l1}^*\right) \tag{56}$$

$$\alpha_{roff}^* = \operatorname{atan2}\left(x_{r2}^*, x_{r1}^*\right) \tag{57}$$

4. Extrinsic Calibration

The aim of extrinsic calibration is the estimation of the position and orientation of the sensor mounted on the robot represented by vector $\mathbf{l}$. As illustrated in [2], extrinsic calibration is formulated as a least-square problem over the constraints derived from equation (6). In particular, the position error on path segment k can be defined as

$$\begin{aligned}\mathbf{e}_{pos}^k &= \left(\mathbf{l}_{pos} + \mathbf{R}\left(l_\theta\right)\boldsymbol{\zeta}_{pos}^k\right) - \left(\boldsymbol{\delta}_{pos}^k + \mathbf{R}\left(\delta_\theta^k\right)\mathbf{l}_{pos}\right) \\ &= \underbrace{\begin{bmatrix} \mathbf{I}_2 - \mathbf{R}\left(\delta_\theta^k\right) & \mathbf{R}\left(\boldsymbol{\zeta}_{pos}^k\right) \end{bmatrix}}_{\mathbf{Q}_k} \underbrace{\begin{bmatrix} \boldsymbol{\varphi}_{pos} \\ \boldsymbol{\varphi}_{ang} \end{bmatrix}}_{\boldsymbol{\varphi}} - \boldsymbol{\delta}_{pos}^k\end{aligned} \tag{58}$$

where $\boldsymbol{\varphi}_{pos} = [\varphi_1, \varphi_2]^\top = [l_x, l_y]^\top$ and $\boldsymbol{\varphi}_{ang} = [\varphi_3, \varphi_4]^\top = [\cos l_\theta, \sin l_\theta]^\top$. Over each path segments the value of $\boldsymbol{\delta}_{pos}^k$ is computed according to eq.(4). The formula holds for both Ackermann and Dual Drive models using the proper values of curvature radius r_κ^k. The vector $\boldsymbol{\varphi}_{ang}$ is subject to constraint $\boldsymbol{\varphi}_{ang}^\top\boldsymbol{\varphi}_{ang} = 1$ to satisfy trigonometric consistency that can be written as

$$h(\boldsymbol{\varphi}) = \boldsymbol{\varphi}^\top \underbrace{\begin{bmatrix} 0 & 0 \\ 0 & \mathbf{I}_2 \end{bmatrix}}_{\mathbf{W}} \boldsymbol{\varphi} - 1 \tag{59}$$

The error function can be chosen in order both to properly represent a distance from the consistent estimation and to allow the computation of its minimum. Such function must depend on all the measurements collected by the robot, while moving along the n path segments. Although more complex functions could weigh the different components of $\mathbf{e}_{pos}^k$, it is convenient to use the square

sum function defined as

$$\begin{aligned} E(\boldsymbol{\varphi}) &= \sum_{k=1}^{n} \mathbf{e}_{pos}^{k\ \top} \mathbf{e}_{pos}^{k} \\ &= \sum_{k=1}^{n} (\boldsymbol{\varphi}^{\top} \mathbf{Q}_k - \boldsymbol{\delta}^{k}{}_{pos})^{\top} (\mathbf{Q}_k\ \boldsymbol{\varphi} - \boldsymbol{\delta}_{pos}^{k}) \\ &= \boldsymbol{\varphi}^{\top} \mathbf{M}_{\varphi} \boldsymbol{\varphi} - 2\boldsymbol{\varphi}^{\top} P_{\varphi} + \left(\sum_{k=1}^{n} \boldsymbol{\delta}_{pos}^{k\ \top}\ \boldsymbol{\delta}_{pos}^{k} \right) \end{aligned} \tag{60}$$

where

$$\mathbf{M}_{\varphi} = \sum_{k=1}^{n} Q_k^{\top}\ Q_k = \begin{bmatrix} m_1 & 0 & m_2 & -m_3 \\ 0 & m_1 & m_3 & m_2 \\ m_2 & m_3 & m_4 & 0 \\ -m_3 & m_2 & 0 & m_4 \end{bmatrix} \tag{61}$$

$$m_1 = \sum_{k=1}^{n} 2(1 - \cos \delta_{\theta}^{k}) \tag{62}$$

$$m_2 = \sum_{k=1}^{n} \left(\zeta_x^k\ (1 - \cos \delta_{\theta}^{k}) - \zeta_y^k\ \sin \delta_{\theta}^{k} \right) \tag{63}$$

$$m_3 = \sum_{k=1}^{n} \left(\zeta_x^k\ \sin \delta_{\theta}^{k} + \zeta_y^k\ (1 - \cos \delta_{\theta}^{k}) \right) \tag{64}$$

$$m_4 = \sum_{k=1}^{n} \left((\zeta_x^k)^2 + (\zeta_y^k)^2 \right) \tag{65}$$

$$\begin{aligned} \mathbf{P}_{\varphi} &= \sum_{k=1}^{n} \mathbf{Q}_k^{\top}\ \boldsymbol{\delta}_{pos}^{k} = \sum_{k=1}^{n} \begin{bmatrix} (\mathbf{I}_2 - \mathbf{R}^{\top}(\delta_{\theta}^{k}))\ \delta_{pos}^{k} \\ \mathbf{R}^{\top}(\zeta_{pos}^{k})\ \boldsymbol{\delta}_{pos}^{k} \end{bmatrix} \\ &= \begin{bmatrix} p_1 & p_2 & p_3 & p_4 \end{bmatrix}^{\top} \end{aligned} \tag{66}$$

Thus, the extrinsic calibration problem is formulated as follows.

Problem 3 (Extrinsic calibration)**.** *Find the parameter vector* $\boldsymbol{\varphi} \in \mathbb{R}^4$ *that*

$$\begin{aligned} \text{minimize} \quad & E(\boldsymbol{\varphi}) = \boldsymbol{\varphi}^{\top} \mathbf{M}_{\varphi} \boldsymbol{\varphi} - 2\boldsymbol{\varphi}^{\top} \mathbf{P}_{\varphi} + \text{const} \\ \text{s.t.} \quad & h(\boldsymbol{\varphi}) = \boldsymbol{\varphi}^{\top} \mathbf{W}_{\varphi} \boldsymbol{\varphi} - 1 = 0 \end{aligned} \tag{67}$$

Problem 3 can be solved through Lagrange multiplier method, since the KKT conditions hold thanks to Slater's conditions. Moreover, it has a closed-form solution that can be obtained by explicitly expanding the linear system $(\mathbf{M}_{\varphi} - \lambda \mathbf{W})\boldsymbol{\varphi} = \mathbf{P}$ and by substituting the resulting $\boldsymbol{\varphi}$ (as function of multiplier λ) in the constraint $h(\varphi)$. The polynomial equation derived by such substitution is

$$\lambda^2 + b_{\varphi}\lambda + c_{\varphi} = 0 \tag{68}$$

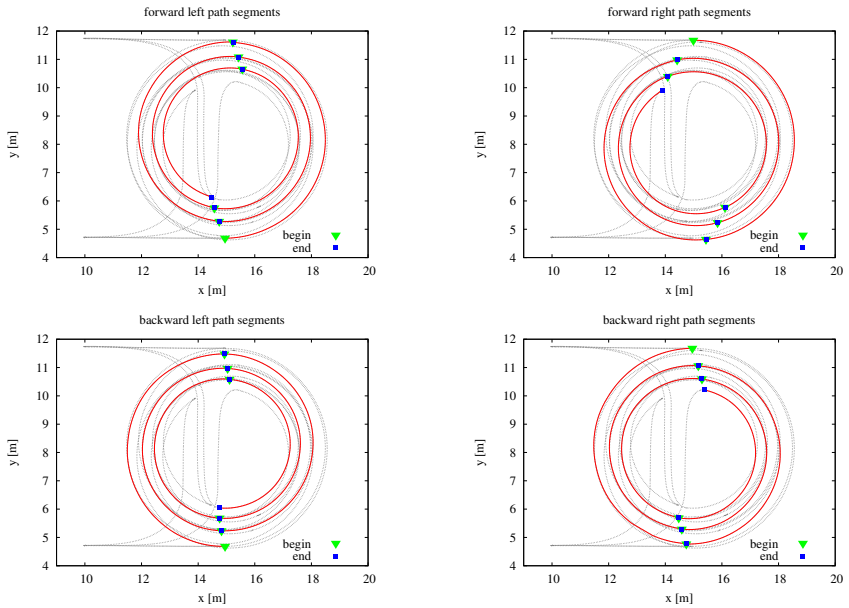

Figure 3: An example of path segments used for calibration with $n_{seg} = 6$ grouped according to versus of direction and steering: forward left segments (top-left), forward right segments (top-right), backward left segments (bottom-left) and backward right segments (bottom-right).

where the coefficients of the equation are

$$b_\varphi = 2\mu_2$$
$$c_\varphi = \mu_2^2 - \frac{(m_1 p_3 - m_2 p_1 - m_3 p_2)^2 + (m_1 p_4 + m_3 p_1 - m_2 p_2)^2}{m_1^2}$$

Each $\lambda_{1,2}$ satisfying equation (68) can be back-substituted into the linear system and the two respective solutions $\boldsymbol{\varphi}^{(1,2)}$ can be obtained. The existence of two solutions is due to the symmetries of the reference equations. The additional physical constraint $\varphi_1 \geqslant 0$ is required to choose between the two outputs [2].

5. From Theory to Practice

The calibration algorithms for Ackermann and Dual Drive kinematics presented in sections 3 and 4 have been implemented and used for calibration of industrial AGVs. The control architecture of the two AGVs has been implemented on PLCs on an embedded computer. PLC systems are widespread and standard industrial solutions to guarantee robustness and real-time execution as well as to comply with safety requirements. Calibration procedures require careful synchronization of data acquired from encoders, laser scanner, sensors and devices in order to relate measurements to the correct segment path, and PLC systems facilitate this task. However, there are some drawbacks in porting

advanced algorithms from laboratory to industrial engineered systems. For example, available PLC library suites provide limited support for advanced data structures, linear algebra and numeric algorithms. The proposed calibration algorithms and the prior formulation of objective functions have been designed taking into account such limitations. Indeed, adopting closed-form solutions is also recommended to cope with such issues of calibration, beside their theoretical importance.

The proposed procedure requires the acquisition of sensor and wheel data while the AGV performs segments of circular paths. For each absolute value of steering angle the system collects four path segments corresponding to left and right steering trajectories, which are travelled in both forward and backward directions. If n_{seg} absolute steering angle values are chosen, then calibration is performed using the corresponding $4n_{seg}$ values. The steering angles of left and right wheels are computed by setting the steering angle of a virtual wheel positioned between the two front wheels. The steering angle α_{wv} of such virtual wheel is varied in the interval $[\alpha_{wv,min}, \alpha_{wv,max}]$. The steering angles α_{wl} and α_{wr} are related to α_{wv} by

$$\tan\alpha_{wl} = \frac{\tan\alpha_{wv}}{1 - \frac{f_y}{f_x}\tan\alpha_{wv}} \qquad \tan\alpha_{wr} = \frac{\tan\alpha_{wv}}{1 + \frac{f_y}{f_x}\tan\alpha_{wv}} \tag{69}$$

The minimum and maximum value of α_{wv} are picked in order to keep the robot in the designated calibration area and to avoid physically impossible values of left and right steering angles. The quadruple of path segment i corresponds to

$$\alpha_{wv}^{k} = \alpha_{wv,min} + \frac{\alpha_{wv,max} - \alpha_{wv,min}}{n_{seg} - 1}\ i \tag{70}$$

where $i = 0, \ldots, n_{seg} - 1$. Positive α_{wv}^{i} lead to left steering circular path segments whereas $-\alpha_{wv}^{i}$ represent the specular right steering segments. While equations (69) hold for both Ackermann and Dual Drive, the minimum and maximum steering values depend on the physical dimensions of the specific robot and on the dimensions of the calibration area.

Thus, the calibration is structured in four phases distinguished by the different combinations of motion direction (forward or backward) and steer angle (towards left or right). During each of these phases the AGV performs circular path segments and gradually increases the (absolute) value of the steering angle α_{wv}, while the curvature radius r_{κ}^{i} decreases. To maintain a regular pattern the path segments are circular arcs with fixed arc length π. Since the robot is not calibrated, the resulting arc lengths only approximate such value. This choice has proven to be the best trade-off to allow sufficiently long trajectories and, at the same time, to reduce the duration of the procedure. In this way the robot approximately covers half-circles while performing the path segments. The velocity for the calibration procedure has been set to 1500 $cdeg/s$, a value that represents the angular velocity of the AGV rigid body around the instant center of rotation. Figure 3 shows an example of path segments used for calibration

with $n_{seg} = 6$ subdivided into four phases according to direction (forward or backward) and steering versus (left or right).

During calibration the correct values of calibration parameters are known only up to their nominal values. Thus, the real trajectories performed for calibrating the robot can be potentially inaccurate. In the developed AGV calibration procedure, the initial nominal values of calibration parameters have been determined as follows. The pose of the laser scanner mounted on the AGV is given by CAD design (usually $l_y = 0$ and $l_\theta = 0$ are assumed) neglecting assembly errors. Driving scales s_{wl} and s_{wr} are assessed from radii and encoder resolution of actuated wheels. Steering offsets α_{loff} and α_{roff} are either assumed to be zero or are set so that the two wheels are approximately parallel and straight. The latter choice limits wheel slipping while the AGV travels along path segments and, thus, enables wheel rotation measurements n^k_{wl} and n^k_{wr} to be more consistent with the real travelled distance.

6. Experiments

The proposed calibration algorithms have been tested on industrial AGVs in warehouse buildings. An Ackermann AGV 17 and a Dual Drive AGV 12, both manufactured by Elettric80 S.p.A., were used in the first two experiments reported henceafter. The proposed calibration method requires forward and backward AGV motions along circular path segments as discussed in section 5. Hence, calibration has been executed in an obstacle-free area able to accommodate circular trajectories with maximum radius of 5 m. These experiments have been designed to assess the correctness and the precision of the proposed calibration method. The goal of the first experiment is the evaluation of the calibration parameters at different calibration conditions. The second experiment estimates the positioning precision of the AGVs at operation points. The third experiment has assessed the position precision and consistency of a fleet of Dual Drive AGVs.

6.1. Calibration Stability Experiments

Due to the unavailability of reliable groundtruth parameters, the stability and robustness of the proposed method are better assessed by repeating the calibration procedure in different settings. Each setting is distinguished by the number of path segments n_{seg} used in the four phases, and by the minimum and maximum values of steering angle α_{wv}. A total of 5 trials have been performed for each setting in order to collect significant statistics. The complete calibration procedure takes about $10 \div 15$ minutes per trial depending on the setting parameters.

Table 1 collects the results achieved in 20 calibrations for Ackermann AGV 17. Most of the trials have been executed using $n_{seg} = 6$ path segments per motion phase, while collecting also the results of shorter calibration with $n_{seg} = 4$. An offset of 0.41 *deg* has been added to all the steering angles α^i_{wv} to satisfy the geometric constraints (available free area, physical limits on steering angles of the AGV, etc.) and to achieve conditions more similar to the tests on

n_{seg}	α_{wv}-min/max [deg]	valid of 5	α_{loff} [cdeg] avg	std	α_{roff} [cdeg] avg	std	s_{wl} [mm/tick] avg	std	s_{wr} [mm/tick] avg	std	l_x [mm] avg	std	l_y [mm] avg	std	l_θ [cdeg] avg	std
6	26.41 ÷ 36.41	5	-207.99	0.21	-291.80	0.40	0.25008	0.00003	0.25013	0.00003	1652.97	0.22	-8.38	0.41	-42.25	0.44
4	26.41 ÷ 41.41	5	-207.98	0.72	-292.62	0.77	0.24982	0.00004	0.24986	0.00005	1652.07	0.21	-6.04	0.92	-39.88	0.87
6	26.41 ÷ 41.41	4	-209.12	1.22	-292.91	1.05	0.25036	0.00016	0.25035	0.00015	1652.74	0.23	-5.07	1.32	-41.71	0.86
6	26.41 ÷ 46.41	4	-208.31	0.43	-292.08	0.51	0.24969	0.00001	0.24972	0.00003	1652.42	0.34	-5.45	0.46	-41.46	0.44

Table 1: Calibration parameters of Ackermann AGV.

n_{seg}	α_{wv}-min/max [deg]	valid of 5	α_{loff} [cdeg] avg	std	α_{roff} [cdeg] avg	std	s_{wl} [mm/tick] avg	std	s_{wr} [mm/tick] avg	std	l_x [mm] avg	std	l_y [mm] avg	std	l_θ [cdeg] avg	std
4	26.00 ÷ 36.00	4	-286.20	0.58	-296.28	0.12	0.24410	0.00023	0.24489	0.00026	560.30	1.96	4.99	2.35	59.08	3.34
6	26.00 ÷ 36.00	4	-286.75	0.46	-295.16	0.37	0.24375	0.00009	0.24453	0.00010	559.82	0.96	4.96	0.92	61.93	1.59
4	26.00 ÷ 41.00	5	-293.82	0.80	-293.86	0.55	0.24363	0.00007	0.24443	0.00007	558.98	0.28	4.69	2.07	61.42	0.46
6	26.00 ÷ 41.00	5	-294.04	1.22	-292.30	0.82	0.24348	0.00006	0.24429	0.00006	559.55	0.74	4.93	1.74	60.36	1.53
4	26.00 ÷ 46.00	5	-296.64	3.00	-291.30	1.44	0.24364	0.00007	0.24448	0.00011	558.66	0.24	4.60	3.20	60.86	0.37
6	26.00 ÷ 46.00	5	-299.76	1.18	-290.60	0.97	0.24406	0.00016	0.24487	0.00017	558.64	0.11	5.05	1.77	61.27	0.91

Table 2: Calibration parameters of Dual Drive AGV.

Dual Drive AGV 12 illustrated in the following. Two outlier estimations have been observed for settings $n_{seg} = 6$ / $\alpha = (26.41 \div 41.41)$ deg and $n_{seg} = 6$ / $\alpha = (26.41 \div 46.41)$. The outlier has been caused by failed sensor registration over one path segment, likely due to insufficient number of detected reflectors. Outlier measurements can be straightforwardly detected by monitoring registration conditions (e.g. checking the number of detected and associated landmarks) and easily dealt with in practical application of the method. The mean value and standard deviation of calibration parameters in Tables 1 and 2 have been computed only from the valid calibration trials. The average values of estimated parameters do not significantly change with the different settings. The sensor coordinate l_y is likely the parameter most sensitive to experimental conditions, as shown by its average values and standard deviation, which is slightly higher than l_x. However, the average value of l_y oscillates at most by 3 mm in different conditions. All the variations on angular parameters are less than 1 deg.

Table 2 illustrates the results achieved in 30 calibrations for Dual Drive AGV 12. Also for Dual Drive two outlier estimations have been observed in sets $n_{seg} = 4$ / $\alpha = (26 \div 36)$ deg and $n_{seg} = 6$ / $\alpha = (26 \div 36)$ deg. Statistics in Table 2 are computed with the exclusion of outlier parameters. The position parameter most sensitive to experimental conditions is again l_y, as shown by its standard deviation. Parameter l_θ, that must be very well calibrated to achieve good AGV movement, has a steady average and a small standard deviation. The values of estimated parameters are stable to different calibration conditions like the number of segments used for calibration or the interval of steering angles. Outliers seem to affect more the estimated value of parameter l_y, whereas the computed values of other parameters are generally comparable to the estimation

		α_{loff} [cdeg]	α_{roff} [cdeg]	s_{wl} [mm/tick]	s_{wr} [mm/tick]	l_x [mm]	l_y [mm]	l_θ [cdeg]
Ackermann AGV	Manual	-200.00	-292.00	0.25483	0.25483	1657.00	0.00	-20.00
	Auto1	-208.43	-292.17	0.25016	0.25017	1652.99	-5.42	-41.02
	Auto2	-208.20	-292.38	0.24968	0.24975	1652.00	-5.94	-41.96
Dual Drive AGV	Manual	-220.00	-298.00	0.24031	0.24031	575.00	12.00	62.00
	Auto1	-292.24	-291.31	0.24350	0.24435	560.24	4.05	58.36
	Auto2	-301.72	-292.24	0.24418	0.24496	558.74	6.68	60.74

Table 3: Calibration parameters used for experiments

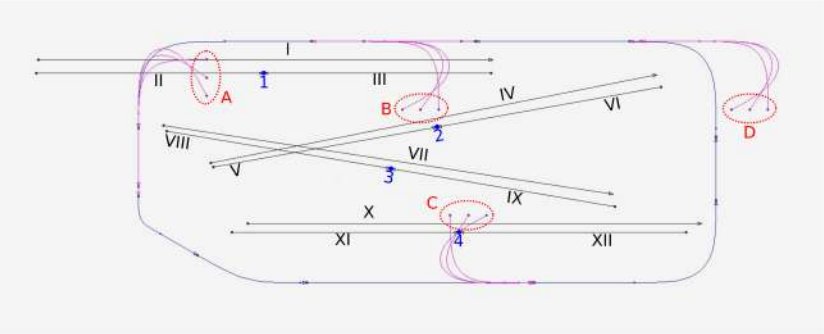

Figure 4: The layout of paths used to perform position precision experiments. The operative area for the vehicle is approx. 16.5 m x 5.5 m

without outliers. Standard deviations decrease with higher number of segments or with larger steering angle interval, although there are some exceptions. Using 6 paths instead of 4 seems to return smaller standard deviations in estimated values. The best set of calibration parameters appears to be the one returned from the tests with $n_{seg} = 6$ / $\alpha = (26 \div 41)$ deg, considering the lack of outliers and the high stability of parameters.

6.2. Position Precision Experiments

Several tasks performed by AGVs require to stop at given operation points of the warehouse, e.g. to load or unload pallets with the forklift. The intrinsic parameters are part of the robot kinematic model and influence both the control system and the odometry. The extrinsic parameters define the pose of the laser scanner used in navigation and localization. An important aim of calibration is to make all the AGVs working in a warehouse stop on the same operation points with adequate precision. Three different sets of experiments have been executed in a real warehouse to evaluate positioning precision obtained by automatic calibration.

1. *Localizer Error.* The first test assesses the distance and heading errors measured by the localizer, when the AGV stops at given operating points. Distance error represent the lateral position error w.r.t. the AGV trajectory terminating on the operating point. These errors depend on AGV navigation and control system and on accuracy of calibration parameters, and cannot be used as groundtruth. However, smaller absolute errors reveal better calibration parameter. We performed this test stopping at operation points placed after either straight or uneven high curvature paths that stress the control system. Straight and curved paths are labelled respectively by roman numerals (I, IV, VII and X) and letters (from A to D) in Figure 4.

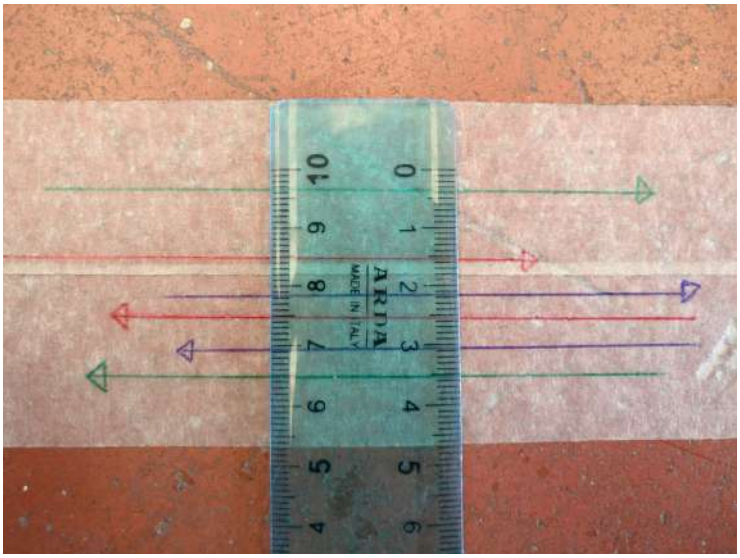

Figure 5: Example of forward and backward paths marked on the ground during the execution of *Straightness Error* test on Ackermann AGV 17. The marker line color identifies the paths obtained using calibration parameters Manual (green), Auto1 (blue) and Auto2 (red).

2. *Straightness Error.* The second test assesses the accuracy of sensor orientation l_θ and, indirectly, of all the other calibration parameters. The AGV moves back and forth over straight paths 10 m long (straight lines with roman numerals I, IV, VII and X in Figure 4). A perfectly calibrated vehicle should execute perfect and overlapping straight trajectories while moving forward and backward. Otherwise, the AGV produces a "leaf shape" moving on slightly different paths when moving forward or backward. The larger is the error on l_θ, the larger is the distance between forward and backward paths. The distance is measured approximately on the medium point of the path by marking the AGV position (the side of its chassis) on the ground as shown in Figure 5.
3. *Halting Point Precision.* The third test evaluates the global quality of calibration parameter set by measuring the halting point precision. The vehicle moves back and forth on two facing straight paths, each 5 m long. In Figure 4, the halting points are labelled with arabic numerals (from 1 to 4), whereas forward and backward paths are in roman numerals. The AGV is manually stopped in the halting point and two points on both sides of back wheels are marked on the ground. This procedure is repeated for both the front facing paths. For example, point 1 is reached from both paths II and III. The halting position of right back wheel from path II is compared with the position of left back wheel on path III (side A), and viceversa (side B). Figure 6 shows an example of marked halting points on the side of an AGV rear wheel.

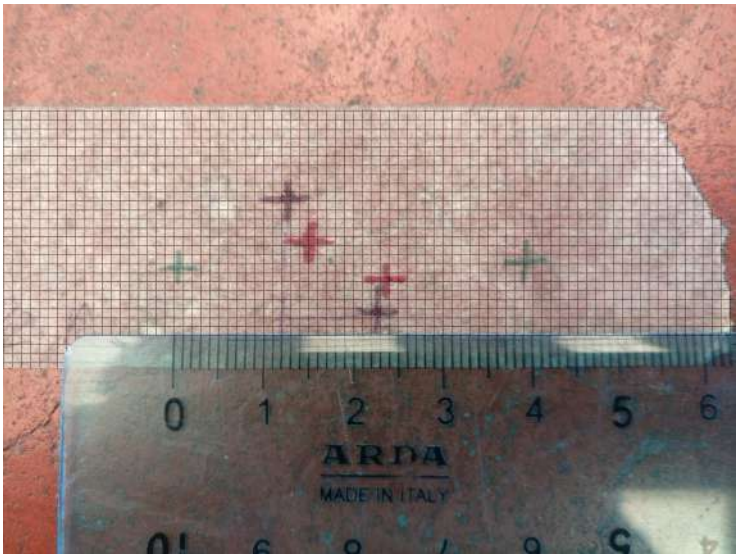

Figure 6: Example of halting points marked on the side of AGV rear wheel during the execution of *Halting Point Precision* test on Dual Drive AGV 12. The marked point color identifies the points obtained using calibration parameters Manual (green), Auto1 (blue) and Auto2 (red).

The three tests have been performed for both Ackermann AGV 17 and Dual Drive AGV 12. For both vehicles, we compared the results obtained with calibration parameter sets *Manual*, *Auto1* and *Auto2* (the latter is not used in some tests) shown in Table 3. As suggested by their name, set *Manual* is obtained through manual calibration performed by an expert operator, whereas *Auto1* and *Auto2* are computed in two different calibration trials of the proposed method for each vehicle type.

The statistical results of the *Localizer Error* test are displayed by the histograms of distance and heading errors in Figure 7(a)-(b) for respectively Ackermann and Dual Drive. Automatic calibration achieves lower average values and standard deviations of distance and heading errors than manual calibration for the two models. The error due to trajectory tracking control is more pronounced on curved paths, but automatic calibration performance is better or comparable.

The *Straightness Error* test has assessed the accuracy of parameter l_θ and, indirectly, of the other calibration parameters. Figure 8(a)-(b) shows the histogram of errors obtained on four straight paths. On Ackermann AGV 17 the automatic calibration procedure always outperforms the manual one. For Dual Drive AGV 12, the straightness error of the calibration parameter sets *Auto1* and *Auto2* is comparable with the one achieved by manual calibration. All trials demonstrate that the value of l_θ has been correctly estimated by manual as well as automatic calibration.

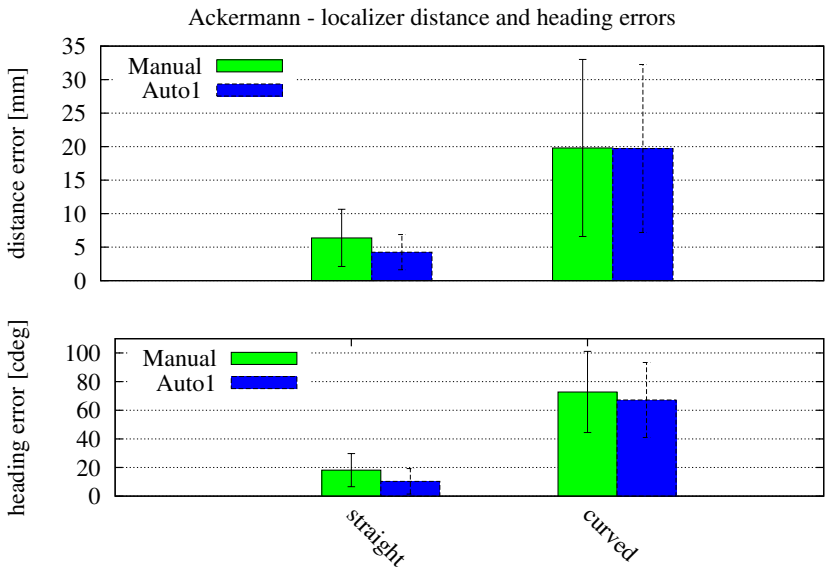

(a)

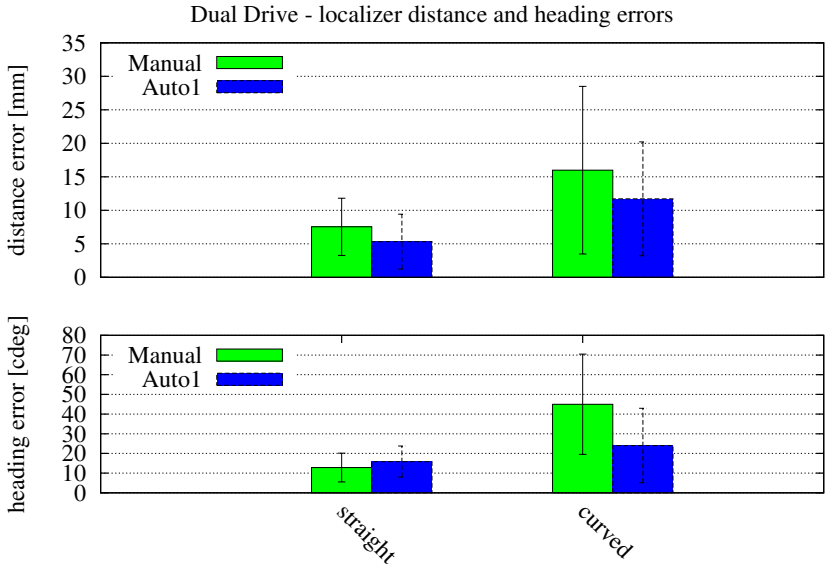

(b)

Figure 7: Results of *Localizer Error* test for Ackerman AGV 17 (a) and Dual Drive AGV 12 on four straight and four curved path segments.

$AGV n^\circ$	α_{loff} [cdeg]	α_{roff} [cdeg]	s_{wl} [mm/tick]	s_{wr} [mm/tick]	l_x [mm]	l_y [mm]	l_θ [cdeg]
1	-325	-286	0.23847	0.23783	554	-8	-18
2	-350	-261	0.23690	0.23720	560	-11	-139
3	-299	-209	0.23703	0.23714	549	-4	-6
4	-369	-244	0.23639	0.23641	548	-2	-44
5	-388	-247	0.23590	0.23620	554	-11	59

Table 4: Calibration parameters of the five Dual Drive AGVs used in fleet position experiments.

In the *Halting Point Precision* test, we measured the precision on halting points reached from two different paths. The distance between the points obtained by the AGV moving on the two facing paths are summarized in Figure 9(a)-(b). For both Ackermann AGV 17 and Dual Drive AGV 12, the automatic calibration procedure achieves lower (or, in the worst cases, similar) distance value between the trail points than the manual one. Parameter computed with the automatic calibration appear to yield more stable and accurate halting points.

6.3. Position Precision of AGV fleets

The results presented in the previous section estimate the position precision achieved by a single AGV when calibrated manually or using the proposed method. Several tasks performed by AGVs require to stop at given operation points of the warehouse, e.g. to load or unload pallets. Position precision depends on different factors including the localization system and the accuracy of calibration. Thus, an important goal of calibration is to make all the AGVs halt at the same points with high precision.

In this section, we report the position precision of a fleet of Dual Drive AGVs operating in a real industrial warehouse. The tests on *straightness error* and *halting point precision* discussed in section 6.2 have been performed on a set of five Dual Drive AGVs calibrated with the proposed method. Table 4 shows the obtained calibration parameters used for each AGV. It can be observed that, although the AGVs are built according to the same design, there are significant variations in both intrinsic and extrinsic parameters and more noticeably in the latter ones. In particular, it is difficult to mechanically mount the laser scanners with the same orientation l_θ.

Figure 10 reports the straighness error of the five AGVs measured for two different straight paths F_I and F_{II}. As usual the straightness error is taken in the middle of the straight path when travelled forward and backward. The measured distance is less than 8 mm for all the AGVs.

Tests on halting point precision have been performed by stopping the robots on two points F_1 and F_2. Each point is reached from two opposite directions and the position error is measured on both the front wheels (sides A and B). The maximum wheel displacement is at most 16 mm. The resulting positional

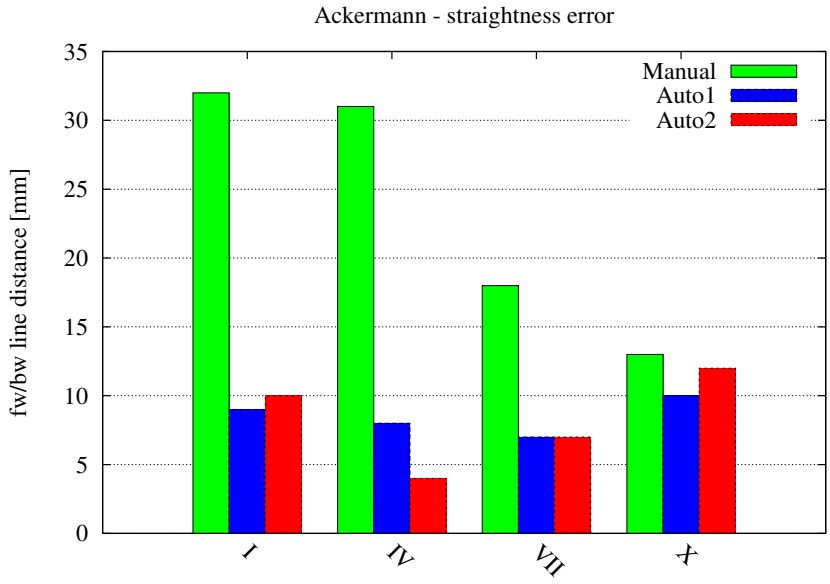

(a)

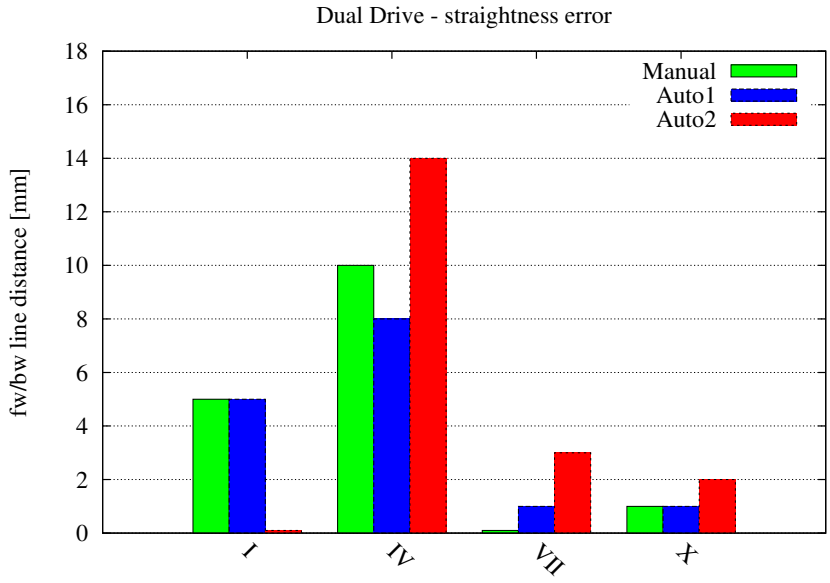

(b)

Figure 8: Results of *Straightness Error* test for Ackerman AGV 17 (a) and Dual Drive AGV 12 (b) on four straight segments labelled by roman numerals as in Figure 4.

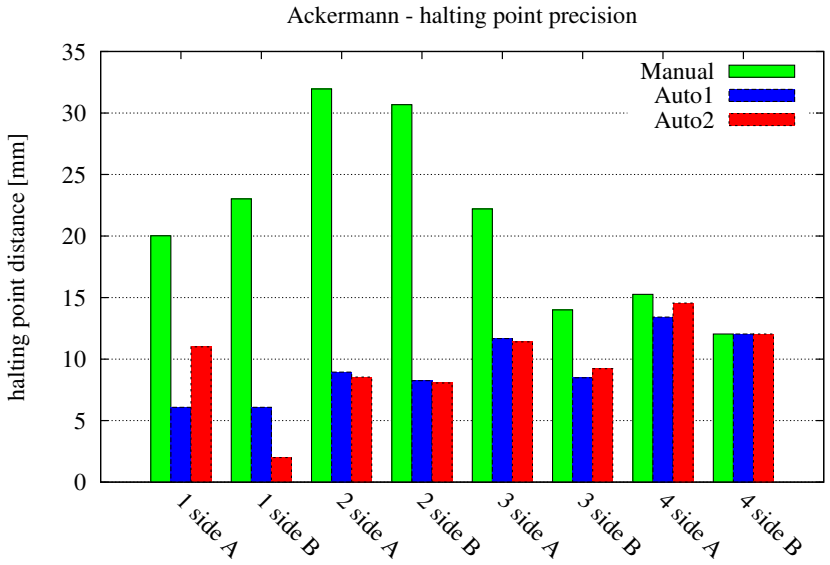

(a)

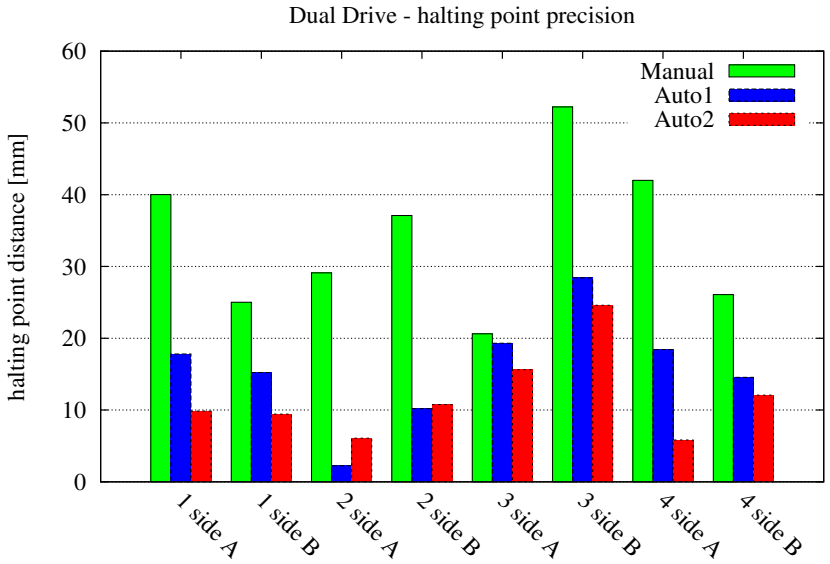

(b)

Figure 9: Results of *Halting Point Precision* test for Ackermann AGV 17 (a) and Dual Drive AGV 12 (b) on four halting points 1, 2, 3 and 4 in Figure 4.

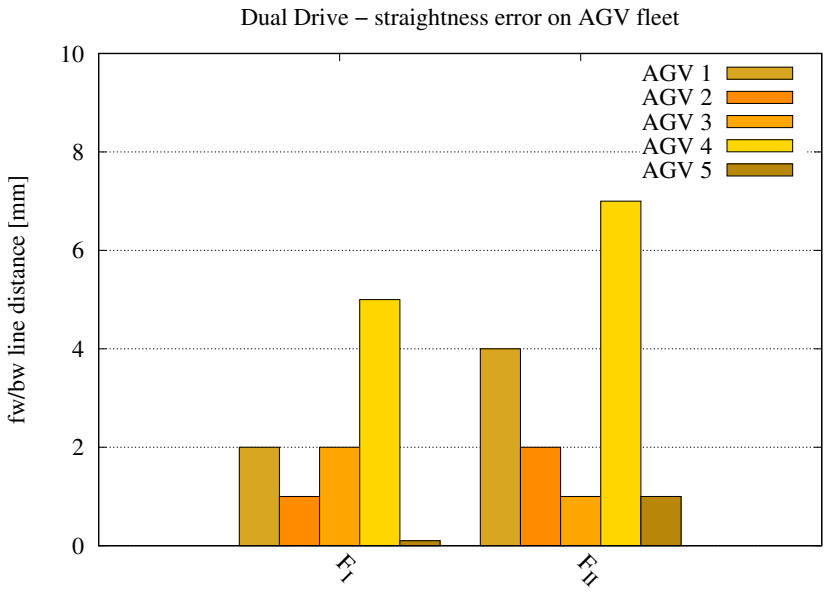

Figure 10: Results of *Straightness Error* test for for a fleet of 5 Dual Drive AGVs on two straight paths F_I and F_{II} in an industrial warehouse.

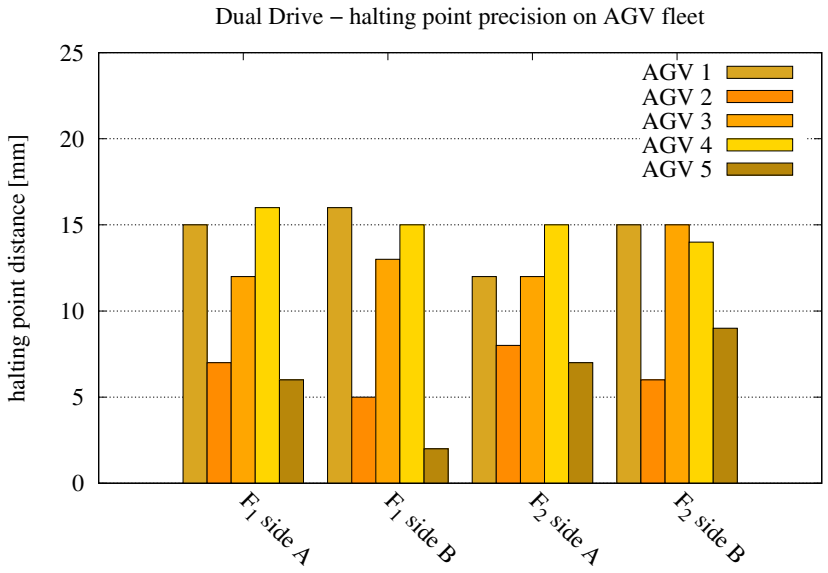

Figure 11: Results of *Halting Point Precision* test for a fleet of 5 Dual Drive AGVs on two halting points F_1 and F_2 in an industrial warehouse.

accuracy is sufficient for correct pallet loading and unloading operations. Indeed, the proposed automatic procedure has consistently calibrated AGVs, enabling them to perform their tasks with equivalent accuracy in a real industrial plant.

7. Conclusion

In this paper, we have proposed a novel method for extrinsic and intrinsic automatic calibration of four wheel industrial AGVs compliant with Ackermann and Dual Drive kinematics. The algorithm estimates the trajectories measured by an onboard sensor and the expected ones given by the state of the wheels. By means of the model equations derived for the specific kinematics, both intrinsic and extrinsic calibration parameters are computed through closed-form solutions of least-square optimization. The methods have been implemented on PLC controllers and experiments have been carried out with industrial AGVs in a warehouse. The precision of the estimated AGV parameters in repeated calibration trials is at most 0.1 deg for angular parameters and typically less than 5 mm for position parameters. The accuracy can be improved by a proper selection of the path segment executed by the AGV and by a manual straightening/parallelization of wheels. The AGVs calibrated with the proposed methods have shown the ability to stop at the same operation points with a typical accuracy of $10 \div 15$ mm if the control system is not overstressed. The experiments on a fleet of AGVs show that the vehicles calibrated with the proposed method achieve adequate similar position precision. This level of position accuracy is comparable with the accuracy obtained with the best manual calibration available in industrial environment. With the suggested number of path segments the automatic calibration procedure takes about 15 minutes for each AGV instead of more than one hour required by the manual iterative procedure. The availability of an automatic, fast and reliable calibration procedure allows more frequent recalibration and hence better AGV localization and navigation performance.

Acknowledgments

This work stems from an ongoing collaboration between Elettric80 S.p.a. and the Department of Engineering and Architecture of the University of Parma.

References

[1] A. Censi, A. Franchi, L. Marchionni, G. Oriolo, Simultaneous calibration of odometry and sensor parameters for mobile robots, IEEE Trans. on Robotics 29 (2). doi:10.1109/TRO.2012.2226380.

[2] F. Kallasi, D. Lodi Rizzini, F. Oleari, M. Magnani, S. Caselli, A novel calibration method for industrial AGVs, Robotics and Autonomous Systems (RAS) 94 (2017) 75–88, dOI 10.1016/j.robot.2017.04.019. doi:10.1016/j.robot.2017.04.019.

[3] J. Borenstein, L. Feng, Measurement and correction of systematic odometry errors in mobile robots, IEEE Transactions on Robotics and Automation 12 (6) (1996) 869–880. doi:10.1109/70.544770.

[4] T. Larsen, M. Bak, N. Andersen, O. Ravn, Location estimation for an autonomously guided vehicle using an augmented Kalman filter to autocalibrate the odometry, in: Proc. Int. Conf. Multisource-Multisens. Inf. Fusion, 1998, pp. 1–6.

[5] A. Martinelli, R. Siegwart, Observability Properties and Optimal Trajectories for On-line Odometry Self-Calibration, in: Proc. of the International Conference on Decision and Control, 2006, pp. 3065–3070.

[6] A. Martinelli, N. Tomatis, R. Siegwart, Simultaneous localization and odometry self calibration for mobile robot, Autonomous Robots 22 (1) (2007) 75–85.

[7] G. Antonelli, S. Chiaverini, G. Fusco, A calibration method for odometry of mobile robots based on the least-squares technique: theory and experimental validation, IEEE Trans. on Robotics 21 (5) (2005) 994–1004.

[8] G. Antonelli, S. Chiaverini, Linear estimation of the physical odometric parameters for differential-drive mobile robots, Journal of Autonomous Robots 23 (1) (2007) 59–68. doi:10.1007/s10514-007-9030-2.

[9] N. Seegmiller, F. Rogers-Marcovitz, G. Miller, A. Kelly, Vehicle model identification by integrated prediction error minimization, Int. Journal of Robotics Research 32 (8) (2013) 912–931.

[10] K. Lee, W. Chung, Calibration of kinematic parameters of a Car-Like Mobile Robot to improve odometry accuracy, in: Proc. of the IEEE Int. Conf. on Robotics & Automation (ICRA), 2008, pp. 2546–2551. doi:10.1109/ROBOT.2008.4543596.

[11] M. De Cecco, Self-calibration of AGV inertial-odometric navigation using absolute-reference measurements, in: Proc. IEEE Instrumentation and Measurement Technology Conference (IMTC), Vol. 2, 2002, pp. 1513–1518 vol.2. doi:10.1109/IMTC.2002.1007183.

[12] P. Goel, S. Roumeliotis, G. Sukhatme, Robust localization using relative and absolute position estimates, in: Proc. of the IEEE/RSJ Int. Conf. on Intelligent Robots and Systems (IROS), 1999, pp. 1134–1140.

[13] J. Kang, W.-S. Choi, S.-Y. An, S.-Y. Oh, Augmented EKF based SLAM method for improving the accuracy of the feature map, in: Proc. of the IEEE/RSJ Int. Conf. on Intelligent Robots and Systems (IROS), 2010, pp. 3725–3731. doi:10.1109/IROS.2010.5652938.

[14] E. Foxlin, Generalized architecture for simultaneous localization, auto-calibration, and map-building, in: Proc. of the IEEE/RSJ Int. Conf. on Intelligent Robots and Systems (IROS), Vol. 1, 2002, pp. 527–533. doi:10.1109/IRDS.2002.1041444.

[15] O. Faugeras, G. Toscani, Camera calibration for 3-D computer vision, in: Proc. Int. Work. Industrial Applications of Machine Vision and Machine Intelligence, 1987, pp. 240–247.

[16] P. Liang, Y. Chang, S. Hackwood, Adaptive self-calibration of vision-based robot systems, Systems, Man and Cybernetics, IEEE Trans. on 19 (4) (1989) 811–824.

[17] T. Sasaki, H. Hashimoto, Calibration of laser range finders based on moving object tracking in Intelligent Space, in: Int. Conf. on Networking, Sensing and Control (ICNSC), 2009, pp. 620–625. doi:10.1109/ICNSC.2009.4919349.

[18] J. Song, G.-I. Jee, Kalman filter based on-line calibration of laser scanner for vehicle navigation, in: Control, Automation and Systems (ICCAS), 2011 11th International Conference on, 2011, pp. 1437–1441.

[19] A. Martinelli, D. Scaramuzza, R. Siegwart, Automatic self-calibration of a vision system during robot motion, in: Proc. of the IEEE Int. Conf. on Robotics & Automation (ICRA), 2006, pp. 43–48. doi:10.1109/ROBOT.2006.1641159.

[20] F. Mirzaei, S. Roumeliotis, A Kalman Filter-Based Algorithm for IMU-Camera Calibration: Observability Analysis and Performance Evaluation, IEEE Trans. on Robotics 24 (5) (2008) 1143–1156. doi:10.1109/TRO.2008.2004486.

[21] Z. Zhang, A flexible new technique for camera calibration, IEEE Trans. on Pattern Analysis and Machine Intelligence 22 (11) (2000) 1330–1334. doi:10.1109/34.888718.

[22] R. Tsai, R. Lenz, A new technique for fully autonomous and efficient 3D robotics hand/eye calibration, IEEE Trans. on Robotics and Automation 5 (3) (1989) 345–358. doi:10.1109/70.34770.

[23] R. Horaud, F. Dornaika, Hand-eye Calibration, Int. Journal of Robotics Research 14 (3) (1995) 195–210.

[24] B. Schmidt, L. Wang, Automatic work objects calibration via a globallocal camera system, Robotics and Computer-Integrated Manufacturing 30 (6) (2014) 678 – 683. doi:10.1016/j.rcim.2013.11.004.

[25] Q. Zhang, R. Pless, Extrinsic calibration of a camera and laser range finder (improves camera calibration), in: Proc. of the IEEE/RSJ Int. Conf. on Intelligent Robots and Systems (IROS), 2004, pp. 2301–2306.

[26] N. Roy, S. Thrun, Online self-calibration for mobile robots, in: Proc. of the IEEE Int. Conf. on Robotics & Automation (ICRA), Vol. 3, 1999, pp. 2292–2297. doi:10.1109/ROBOT.1999.770447.

[27] A. Kelly, Linearized Error Propagation in Odometry, Int. Journal of Robotics Research 23 (2) (2004) 179–218.

[28] D. Cucci, M. Matteucci, A Flexible Framework for Mobile Robot Pose Estimation and Multi-Sensor Self-Calibration, in: Proc. of the Intl. Conf. on Informatics in Control, Automation and Robotics (ICINCO), 2013, pp. 1–8.

[29] J. Underwood, A. Hill, T. Peynot, S. Scheding, Error modeling and calibration of exteroceptive sensors for accurate mapping applications, Journal of Field Robotics 27 (1) (2010) 2–20. doi:10.1002/rob.20315.

[30] J. Brookshire, S. Teller, Automatic calibration of multiple coplanar sensors, in: Robotics: Science and Systems, MIT Press, 2011, pp. 33–40.

[31] J. Brookshire, S. Teller, Extrinsic Calibration from Per-Sensor Egomotion, in: Robotics: Science and Systems, MIT Press, 2012, pp. 25–32.

[32] D. Lodi Rizzini, F. Kallasi, J. Aleotti, F. Oleari, S. Caselli, Integration of a Stereo Vision System into an Autonomous Underwater Vehicle for Pipe Manipulation Tasks, Computers and Electrical Engineering (CAEE) 58 (2017) 560–571, dOI 10.1016/j.compeleceng.2016.08.023, EID 2-s2.0-84994797689. doi:10.1016/j.compeleceng.2016.08.023.

[33] X. Wu, Y. Zhang, T. Zou, L. Zhao, P. Lou, Z. Yin, Coordinated path tracking of two vision-guided tractors for heavy-duty robotic vehicles, Robotics and Computer-Integrated Manufacturing 53 (2018) 93 – 107. doi:10.1016/j.rcim.2018.03.012.

[34] G. Vasiljevic, D. Miklic, I. Draganjac, Z. Kovaic, P. Lista, High-accuracy vehicle localization for autonomous warehousing, Robotics and Computer-Integrated Manufacturing 42 (2016) 1 – 16. doi:10.1016/j.rcim.2016.05.001.

[35] H. Martnez-Barberà, D. Herrero-Pèrez, Autonomous navigation of an automated guided vehicle in industrial environments, Robotics and Computer-Integrated Manufacturing 26 (4) (2010) 296 – 311. doi:10.1016/j.rcim.2009.10.003.

[36] P. McKerrow, D. Ratner, Calibrating a 4-wheel mobile robot, in: Proc. of the IEEE/RSJ Int. Conf. on Intelligent Robots and Systems (IROS), 2002, pp. 859–864.

[37] D. Hess, F. Kuenemund, C. Roehrig, Simultaneous calibration of odometry and external sensors of omnidirectional automated guided vehicles (agvs), in: International Symposium on Robotics (ISR), 2016, pp. 480–487.

[38] J. Maye, H. Sommer, G. Agamennoni, R. Siegwart, P. Furgale, Online self-calibration for robotic systems, Int. Journal of Robotics Research 35 (4) (2016) 357–380. doi:10.1177/0278364915596232.

[39] F. Kallasi, D. Lodi Rizzini, Efficient Loop Closure based on FALKO LIDAR Features for Online Robot Localization and Mapping, in: Proc. of the IEEE/RSJ Int. Conf. on Intelligent Robots and Systems (IROS), 2016, pp. 1206–1213.

[40] A. Kelly, N. Seegmiller, A vector algebra formulation of mobile robot velocity kinematics, in: Field and Service Robotics, Springer, 2014, pp. 613–627.

[41] R. Hartley, A. Zisserman, Multiple View Geometry in Computer Vision, 2nd Edition, Cambridge University Press, 2004.